Internet Electronic Journal of Molecular Design **2003**, *2*, 000–000
BioChem Press http://www.biochempress.com

Periodic Table of Carbon Nanotubes Based on the Chiral Vector

Francisco Torrens,*

Institut Universitari de Ciència Molecular, Universitat de València, Dr. Moliner 50, E-46100 Burjassot (València), Spain

Received xxx; Preprint published xxx; Accepted xxx ; Published xxx

Internet Electron. J. Mol. Des. **2003**, *1*, 000–000

Abstract

Motivation. The periodic table (PT) of the elements suggests that hydrogen could be the origin of everything. *The construction principle is an evolutionary process that is formally similar to those of Darwin and Oparin*. The PT of fullerenes suggests that C_{60} could be the origin of fullerenes and C_{30} could be considered as the element zero of such a PT.

Method. The elementary polarizabilty per atom $<\alpha>$ is calculated with the interacting induced-dipole polarization model implemented in program PAPID.

Results. The polarizabilty $<\alpha>$ of single-wall carbon nanotubes (SWNT) is related to the indices (*n*,*m*) designating the *chiral vector*. SWNTs are classified in *zigzag* (*n*,0), *armchair* (*n*,*n*) and *chiral* (*n*,*m*). The $<\alpha>$ allows classifying SWNTs according to the chiral vector indices (*n*,*m*). A format is recommended for the PT of SWNTs.

Conclusions. The periodic law has not the rank of the laws of physics. (1) The properties of SWNTs are not repeated. (2) The order relationships show exceptions. The proposed statement is: *The relationships that any SWNT* (n,m) *has with its neighbour* (n-1,m+1) *are approximately repeated for each period*. Semifullerenes could be the origin of SWNTs and they could be considered as the element zero of the PT. The correlation between $<\alpha>$ and $(n^2+nm+m^2)^{1/2}$ shows that the vector indices (*n*,*m*) are adequate. The most interesting combination is $(n^2+nm+m^2)^{1/2}$. The (10,10) presents a consistency between a relatively small $<\alpha>$ and great kinetic stability.

Availability. The original software used in the investigation is available from the author.

Keywords. Periodic table; carbon nanotube; polarizability; interacting induced-dipole polarization; electrical property; nanostructure.

Abbreviations and notations

2D, two-dimensional	PT, periodic table
3D, three-dimensional	SWNT, single-wall carbon nanotube
ECEPP, empirical conformational energy program for peptides	SWNTHC, single-wall carbon nanotube hydrocarbon
H, hydrogen	v, number of vertices
MM, molecular mechanics	v_2, number of divalent vertices
p, position in the periodic table	v_3, number of trivalent vertices
PL, periodic law	

1 INTRODUCTION

The periodic table (PT) of the elements [1] suggests that hydrogen (H) could be the origin of everything else. In addition to H they are neutrons, which can be considered as the element zero of the PT. *The construction principle is an evolutionary process* applied to atomic species. Inspired by the PT of the elements, several PTs can be suggested: of relativistic effects [2] and molecules, *e.g.*,

* Correspondence author; phone: 34-963-543-182; fax: 34-963-543-156; E-mail: Francisco.Torrens@uv.es

Copyright © 2003 BioChem Press

alkanes [3,4], acyclic hydrocarbons [5,6], polycyclic aromatic hydrocarbons [7,8], benzenoid hydrocarbons [9], fullerenes [10], C_{60} fullerenes [11], helicenes [12] and drugs [13].

The growth mechanism of single-wall carbon nanotubes (SWNT) is complex. Why do SWNTs form in the first place at high temperatures when they are not thermodynamically the most stable structures? Smalley suggested that the high electric field, due to the voltage drop in the space-charge sheath near the cathode, might be responsible for keeping SWNTs open and might result in elongated structures [14]. More detailed analysis of the physics of the arc plasma by Gamaly and Ebbesen indicated that the electric field is not the major player, and the growth of SWNTs is the result of the competition between two types of carbon species present near the cathode: the anisotropic unidirectional carbon ions accelerated across the gap, and the thermally evaporated carbon from the cathode with isotropic velocity distribution [15]. Self-assembly of fullerenes [16] and SWNTs is a sharp demonstration of the classical crystal physics of *nucleation and growth*. In a graphite-rod arc discharge [17] or during laser ablation [18], energetic C atoms comprising a dense neutral *gas* ($T \geq T_F \sim 5600$K) undergo repeated nearest-neighbour collisions, which become more *sticky* during normal three-dimensional (3D) system cooling [19]. In this vapour process of homogeneous C_{60} nucleation colliding C_1, C_2, C_3 *etc*. are ultimately self-trapped into transient growing molecular C_n nuclei, whose size and architectural form are essentially determined by the fundamental C–C bond. In a time ~2500ps an essentially two-dimensional (2D) pentagon becomes the base for a corannulene (C_{20}) *bowl* in 3D [20], developing swiftly by edge/step accretion into a *hemisphere* (C_{30}), which then finally rapidly closes into the truncated icosahedron of C_{60}. Chadderton and Chen grew controllably SWNTs and other nanoclusters by simple surface self-diffusion, both homogeneously and heterogeneously, following a mechanical ball-milling preparative stage [21]. Thess *et al*. produced fullerenic SWNTs by condensation of a laser-vaporized C-Ni-Co mixture at 1200ºC [22]. X-ray diffraction and electron microscopy showed that these SWNTs are nearly uniform in diameter and that they self-organize into *ropes*, which consist of 100–500 SWNTs in a 2D triangular lattice with a lattice constant of 17Å. The X-ray form factor is consistent with that of uniformly charged cylinders 13.8±0.2Å in diameter. The ropes were metallic, with a single-rope resistivity of $<10^{-4}\Omega\cdot$cm at 300K. The uniformity of SWNT diameter is attributed to the efficient annealing of an initial fullerenic tubelet kept open by a few metal atoms; the optimum diameter is determined by competition between the strain energy of curvature of the graphene sheet and the dangling-bond energy of the open edge, where growth occur. These factors strongly favour the metallic (10,10) SWNT with C_{5v} symmetry and an open edge stabilized by triple bonds.

The simplest way of specifying the structure of a SWNT is in terms of the *chiral* vector, **C**, which is the lattice vector joining two equivalent points on the original graphene lattice. The cylinder is produced by rolling the sheet such that the two end-points of the vector are superimposed. Because of the symmetry of the honeycomb lattice, many of the cylinders produced

in this way will be equivalent, but there is an *irreducible wedge* comprising one twelfth of the graphene lattice, within which unique SWNT structures are defined. Each pair of integers (*n*,*m*) represents a possible SWNT structure. Thus the vector **C** can be expressed as $\mathbf{C} = n\,\mathbf{a}_1 + m\,\mathbf{a}_2$, where $\mathbf{a}_1$ and $\mathbf{a}_2$ are the unit cell base vectors of the graphene sheet, and $n \geq m$. SWNTs can be classified in three types: (1) *zigzag* ($m = 0$), by the form of their edge, (2) *armchair* ($n = m$), where the edge presents the form of an armchair and (3) *chiral* (*n*,*m*), where the hexagons are arranged helically around the SWNT axis. Since $|\mathbf{a}_1| = |\mathbf{a}_2| = 2.46$Å, the magnitude of **C** in angstroms is $2.46(n^2+nm+m^2)^{1/2}$, and the diameter is given by $d_t = \mathbf{C}/\pi = 0.783(n^2+nm+m^2)^{1/2}$. When $n - m = 3q$, where q is an integer, the SWNT is metallic or semimetallic, and the remaining species are semiconducting with a geometry-dependent bandgap. In previous works, a PT of fullerenes was presented [23,24]. In the present report the polarizability of SWNTs is calculated with the aim of classifying SWNTs. Section 2 presents the method. Section 3 describes the improvements. Section 4 discusses the results. Section 5 summarizes the conclusions.

2 MATERIALS AND METHODS

The molecular polarizability, $\alpha_{ab}^{\mathrm{mol}}$, is defined as the linear response to an external electric field,

$$\mu_a^{\mathrm{ind}} = \alpha_{ab}^{\mathrm{mol}} E_b^{\mathrm{ext}} \tag{1}$$

where μ_a^{ind} is the induced molecular dipole moment and *a*, *b*, *c*… denote Cartesian components. Considering a set of N interacting atomic polarizabilities, the atomic induced dipole moment has a contribution also from the other atoms,

$$\mu_{p,a}^{\mathrm{ind}} = \alpha_{p,ab}\left(E_b^{\mathrm{ext}} + \sum_{q\neq p}^{N} T_{pq,bc}^{(2)}\mu_{q,c}^{\mathrm{ind}}\right) \tag{2}$$

where $T_{pq,bc}^{(2)}$ is the interaction tensor

$$T_{pq,ab}^{(2)} = \frac{3r_{pq,a}r_{pq,b}}{r_{pq}^5} - \frac{\delta_{ab}}{r_{pq}^3} \tag{3}$$

where r_{pq} is the distance between atoms p and q, and δ represents the Kronecker delta function: $\delta(\square,\square) = 1$ if $\square = \square$, and $\delta(\square,\square) = 0$ if $\square \neq \square$. The molecular polarizability can then be written as

$$\alpha_{ab}^{\mathrm{mol}} = \sum_{p}^{N}\alpha_{p,ab}^{\mathrm{eff}} = \sum_{q,p}^{N} B_{pq,ab} \tag{4}$$

where $\alpha_{\square}^{\mathrm{eff}}$ is the effective polarizability of atom p and **B** is the relay matrix defined as (in a supermatrix notation)

$$\mathbf{B} = \left(\alpha^{-1} - T^{(2)}\right)^{-1} \tag{5}$$

The atomic parameters $\alpha_{\square}$ have previously been fitted to the full polarizability tensors of quantum-mechanical computed molecular polarizabilities of a series of 115 substituted aliphatic and aromatic molecules containing the elements H, C, N, O, F and Cl.

3 IMPROVEMENTS IN THE POLARIZATION MODEL

The following improvements have been implemented in the model.

1. In order to build the relay matrix **B**, the atomic polarizability tensor $\boldsymbol{\alpha}_{\square} = \boldsymbol{\alpha}_{\square}{}^{\sigma} + \boldsymbol{\alpha}_{\square}{}^{\pi}$ has been used instead of the scalar polarizability $\alpha_{\square}$. The σ atomic polarizability tensor is calculated according to:

$$\boldsymbol{\alpha}^{\sigma} = \sum_{\text{bonds}} \frac{3\alpha^{\sigma}}{\alpha_{\parallel}^{\sigma} + 2\alpha_{\perp}^{\sigma}} \begin{bmatrix} \alpha_{\perp}^{\sigma} & 0 & 0 \\ 0 & \alpha_{\perp}^{\sigma} & 0 \\ 0 & 0 & \alpha_{\parallel}^{\sigma} \end{bmatrix} = \sum_{\text{bonds}} \frac{3\alpha^{\sigma}}{3.676} \begin{bmatrix} 1 & 0 & 0 \\ 0 & 1 & 0 \\ 0 & 0 & 1.676 \end{bmatrix} \tag{6}$$

where the *z*-axis is defined as the bond direction for each bond. The diagonal form of $\boldsymbol{\alpha}^{\sigma}$ has two distinct components noted as $\alpha^{\sigma}_{\parallel}$ and $\alpha^{\sigma}_{\perp}$, parallel and perpendicular to the bond axis, respectively. The parameter $\alpha^{\sigma}_{\parallel}/\alpha^{\sigma}_{\perp} = 1.676$ has been obtained fitting isotropic bonding polarizabilities. The π atomic polarizability tensor is calculated as:

$$\boldsymbol{\alpha}^{\pi} = \sum_{\text{bonds}} \frac{3\alpha^{\pi}}{2\alpha_{\parallel}^{\pi} + \alpha_{\perp}^{\pi}} \begin{bmatrix} \alpha_{\parallel}^{\pi} & 0 & 0 \\ 0 & \alpha_{\parallel}^{\pi} & 0 \\ 0 & 0 & \alpha_{\perp}^{\pi} \end{bmatrix} = \sum_{\text{bonds}} \frac{3\alpha^{\pi}}{3.741} \begin{bmatrix} 1 & 0 & 0 \\ 0 & 1 & 0 \\ 0 & 0 & 1.741 \end{bmatrix} \tag{7}$$

2. Damping functions have been used in the calculation of the interaction tensor to prevent the polarizability from going to infinity. Thole proposed

$$T^{(2)}_{pq,ab} = \frac{3v^4_{pq} r_{pq,a} r_{pq,b}}{r^5_{pq}} - \frac{\left(4v^3_{pq} - 3v^4_{pq}\right)\delta_{ab}}{r^3_{pq}} \tag{8}$$

where $v_{pq} = r_{pq}/s_{pq}$ if $r_{pq} < s_{pq}$; otherwise $v_{pq} = 1$ [25]. The term s is defined as $s = 1.662(\alpha_p \alpha_q)^{1/6}$. Miller proposed

$$T^{(2)}_{pq,ab} = \left[\frac{3r_{pq,a} r_{pq,b}}{r^5_{pq}} - \frac{\delta_{ab}}{r^3_{pq}}\right]\left\{1 - \exp\left[-\left(\frac{r_{pq}}{0.7\rho_{pq}}\right)^{10}\right]\right\} \tag{9}$$

with $\rho_{pq} = \rho_p + \rho_q$ (sum of the van der Waals radii) [26].

3. The interactions between bonded atoms and between atoms within a distance lying in an interval defined by $[r^{\text{inf}}, r^{\text{sup}}]$ have been neglected. The starting values for this interval are $[0, 10^{30}]$ and r^{inf} is incremented if resonance conditions are detected.

4. Two tests indicating a resonance condition have been implemented: test whether matrix $\mathbf{B}^{-1}$ is singular and whether matrix $\mathbf{B}^{-1}$ is not positive definite.

An optimized version of program PAPID [27] including the whole interacting induced dipole polarization model has been implemented in the program molecular mechanics (MM2) [28], its extension to transition metals (MMX) [29] and the empirical conformational energy program for peptides (ECEPP2) [30]. The new versions are called MMID2 [31], MMXID [32] and ECEPPID2

[33].

4 RESULTS AND DISCUSSION

Table 1. Elementary Polarizabilities as a Function of Radius R for (*n*,0) Zigzag and (*n*,*n*) Armchair Nanotubes.

Number of atoms	*R* (Å)	$<\alpha>$ (Å^3)[a]	Jensen *et al*.[b]
16 (4,0)	1.633	1.300	–
20 (5,0)	2.050	1.281	–
24 (6,0)	2.330	1.286	–
28 (7,0)	2.784	1.308	–
32 (8,0)	3.198	1.333	–
36 (9,0)	3.543	1.361	–
40 (10,0)	3.798	1.392	–
44 (11,0)	4.297	1.423	–
48 (12,0)	4.755	1.453	–
52 (13,0)	5.253	1.448	–
56 (14,0)	5.728	1.469	–
60 (15,0)	6.057	1.488	–
64 (16,0)	6.598	1.505	–
68 (17,0)	6.935	1.521	–
72 (18,0)	7.425	1.536	–
76 (19,0)	7.953	1.548	–
80 (20,0)	8.527	1.560	–
∞ (∞,0) (extrapolation)	∞	1.604	–
42 (7,0)	2.771	1.184	–
48 (8,0)	3.083	1.201	–
54 (9,0)	3.515	1.220	–
60 (10,0)	3.907	1.239	–
66 (11,0)	4.214	1.260	–
72 (12,0)	4.904	1.279	–
∞ (∞,0) (extrapolation)	∞	1.428	–
72 (9,0)	3.501	1.132	–
90 (9,0)	3.487	1.130	1.304
100 (10,0)	3.931	1.145	–
110 (11,0)	4.277	1.160	–
120 (12,0)	4.711	1.175	–
130 (13,0)	5.064	1.189	–
140 (14,0)	5.492	1.202	–
150 (15,0)	5.850	1.215	–
160 (16,0)	6.273	1.227	–
170 (17,0)	6.636	1.239	–
180 (18,0)	7.055	1.249	–
∞ (∞,0) (extrapolation)	∞	1.388	–
∞ (∞,0) (∞-long extrapolation)	∞	1.318	–
90 (5,5)	3.390	1.148	1.305
100 (5,5)	3.390	1.136	1.331 (110)
120 (6,6)	4.084	1.158	–
140 (7,7)	4.746	1.179	–
160 (8,8)	5.436	1.200	–
180 (9,9)	6.102	1.219	–
200 (10,10)	6.789	1.237	–
∞ (∞,∞) (extrapolation)	∞	1.348	–

[a] Average dipole-dipole polarizability.

[b] Ab initio SCF/STO-3G calculations taken from Reference 36. Figures in parentheses indicate number of atoms.

Both (*n*,0) zigzag and (*n*,*n*) armchair SWNTs are studied with the number of C atoms varying

from $v = 16$ to 200 for $n = 4$ to 20 [34,35]. Table 1 gives the elementary polarizability per atom $<\alpha>$ for SWNTs. Molecular geometries have been optimized with MMID2. The radius of the SWNT, R, increases with the number of rings around a section of the SWNT, n. In general the calculated $<\alpha>$ increases monotonically with R. For thinner SWNTs $<\alpha>$ is computed smaller for the (n,0) C_{100}–C_{200} than for the (n,n) SWNTs C_{90}–C_{180}. However this trend is reversed after $R = 5.4$Å for the (14,0) and thicker SWNTs. In particular, for the (9,0) SWNT C_{90} the calculated $<\alpha> = 1.130$Å^3 is similar to the reference *ab initio* calculation of $<\alpha> = 1.304$Å^3 by Jensen *et al*. [36]. Moreover the agreement is improved for shorter (9,0) SWNTs as C_{72}, $<\alpha> = 1.132$Å^3, C_{54}, $<\alpha> = 1.220$Å^3, and even C_{36}, $<\alpha> = 1.361$Å^3. The variation of $<\alpha>$ with the radius of the (n,0) zigzag SWNTs C_{90}–C_{180} fits to

$$\frac{1}{\alpha} = a + \frac{b}{R} \tag{10}$$

where □ is the inverse $<\alpha>$ of the graphene. The calculated polarizabilities result

$$\frac{1}{\alpha} = 0.721 + \frac{0.595}{R} \qquad N = 10 \quad r = 0.992 \quad s = 0.004 \quad F = 520.6 \tag{11}$$

and $<\alpha>$ for the graphene plane extrapolates as 1.388Å^3. The $<\alpha>$ calculated for the (n,0) SWNTs with $n \leq 8$ deviates from the above simple scaling, perhaps due to the fact that the singlet π^* band, which is normally in the conduction band, falls into the band gap as a result of increased σ^*–π^* mixing at high curvature [37]. While the band gap shows significant change with n, $<\alpha>$ varies smoothly with R^{-1}. Increasing $<\alpha>$ with decreasing R shows that, for small R, the character of the surface deviates from that of the graphene sheet. This finding suggests that, creating regions of different curvature on a single SWNT by radial deformation, one can attain different values of $<\alpha>$. For the (n,n) armchair SWNTs C_{100}–C_{200} the variation of the calculated $<\alpha>$ with R results

$$\frac{1}{\alpha} = 0.742 + \frac{0.485}{R} \qquad N = 6 \quad r = 0.989 \quad s = 0.004 \quad F = 185.1 \tag{12}$$

and $<\alpha>$ for the graphene plane extrapolates as 1.348Å^3. Additional fits are reported in Table 1.

An [n]acene is a planar polybenzenoid formed of n linearly fused benzene rings. An [n]cyclacene is a circular acene formed of n linearly annelated benzene rings. A graph-theoretical study of the (n,0) zigzag SWNT [n]cyclacenes C_{16}–C_{80} has been performed. The determinant of a 3×3 matrix $\mathbf{A} \equiv [a\ b\ c,\ d\ e\ f,\ g\ h\ i]$ is $aei - ahf - dbi + dhc + gbf - gec$. The permanent of this matrix, per(**A**), is the *sum* of the same six terms. For the SWNTs the Kekulé structure count ($K = 2$) is constant, and smaller than for the corresponding planar acenes (naphthacene to eicosacene linear polybenzenoid hydrocarbons with K in the range 5–21). This indicates a smaller stability for the former. Moreover, for the SWNTs the permanent of the adjacency matrix of the hydrogen-suppressed graph [per(**A**) = 16] is also constant, and smaller than for the corresponding planar acenes, per(**A**) in the range 25–441. The ratio per(**A**)/ln$K$ = 2 for alternant hydrocarbons (*e.g*. planar acenes from benzene to eicosacene), and slightly greater for rather delocalized hydrocarbons [*e.g*.

corannulene with per(**A**)/ln$K$ = 2.0136]. However, for the SWNTs per(**A**)/ln$K$ = 4 is constant and greater than for the corresponding planar acenes [per(**A**)/ln$K$ = 2], which confirms the smaller stability for the former. The corresponding interpretation is that in the SWNTs local electron delocalization per C atom is small.

Moreover, the aromaticity for SWNTs is hindered by the pyramidalization angle θ for the C atoms, which decreases from the (4,0) zigzag SWNT (θ = 11.2˚) to the (20,0) SWNT (θ = 2.5˚) and [n]cyclacenes, and becomes 0˚ for the graphene sheet and planar acenes [38]. This is in agreement with the smaller stability for the SWNTs. The interpretation is that the thick SWNTs present a greater global electron delocalization per C atom. This is attributed to the fact that the electron charge of each atom in the thicker SWNTs can be shared with a larger number of atoms. Similar results are shown by the (n,n) armchair SWNTs, which decrease θ from (5,5), θ = 6.0˚, to (10,10), θ = 3.0˚. The pyramidalization angles can be compared with those of fullerenes, which decrease from C_{60}-I_h (12.0˚) to C_{240}-I_h (5.8˚). Although fullerenes and SWNTs are both examples of curved carbon, there are significant structural differences that are expected to be reflected in their chemistry; in particular, fullerenes are curved in 2D, whereas SWNTs are curved in one dimension. Thus for a curved carbon structure of given radius, the C atoms in a fullerene are more distorted than those in the corresponding SWNT, *e.g.*, to curve a graphene sheet into a (10,10) SWNT requires a pyramidalization angle of *ca*. 3.0º, whereas the fullerene of equivalent radius, C_{240} [a (10,10) SWNT can be capped by a hemisphere of C_{240}], has θ = 5.8º. The strain energy of pyramidalization is roughly proportional to θ^2, so the fullerene must absorb *ca*. 10 times the strain energy of pyramidalization per C atom, compared to the *equivalent* SWNT at these diameters.

The results for both graph-theoretical and geometric studies are consistent with the standard heats of formation ΔH_f°, calculated with program MOPAC-AM1. The curve for the (n,0) SWNT hydrocarbon (SWCNHC) [n]cyclacenes $C_{16}H_8$–$C_{48}H_{24}$ is less stable, but converges to that for the planar acenes when the number of vertices v approaches infinity, because the curvature disappears. In order to compare the SWNTHC [n]cyclacenes $C_{16}H_8$–$C_{48}H_{24}$, ΔH_f° per C atom, $\Delta H_f^\circ/v$, has been contrasted. MOPAC-AM1 $\Delta H_f^\circ/v$ shows that the thicker (n,0) SWNTHCs are relatively more stable than the thinner SWNTHCs, which suggests that thicker infinite SWNTs will be relatively more stable than thinner infinite SWNTs. While SWNTHCs are strongly stabilized as v increases, planar acenes are slightly destabilized as v increases. The curve for the planar acenes extrapolates to 27.48kJ·mol^{-1} for v approaching infinity. Moreover, the curve for the SWNTHCs converges to that for the planar acenes when v approaches infinity, because the curvature disappears. This is in correspondence with the calculations of Mitmire's group that, to a good approximation, the strain energy per atom varied with $1/d_t^2$ [39]. For SWNTs with diameters larger than about 16Å, the strain energy becomes rather close to that in planar graphite. This diameter is approximately the same as the smallest observed experimentally in multiwalled nanotubes. They found that strain energy was independent of SWNT structure. The $\Delta H_f^\circ/v$ for the (n,0) SWNTHC [n]cyclacenes $C_{16}H_8$–$C_{48}H_{24}$

correlates with the ratio (number of trivalent vertices)/(number of divalent vertices) v_3/v_2 in the SWNT. For the SWNTHCs, $v_3/v_2 = 1$ is constant and greater than for the corresponding planar acenes (naphthacene to dodecacene v_3/v_2 in the range 0.500–0.786). The extrapolated value of $\Delta H_f^\circ/v_{\mathrm{SWNTHC}}$ for $v_3/v_{2,\mathrm{SWNT}}$ approaching one gives 27.81kJ·mol^{-1}, in agreement with the asymptotic value of the $\Delta H_f^\circ/v$–v plot, 27.48kJ·mol^{-1}.

Table 2. Recommended Format for the Table of Periodic Properties of Nanotubes Based on the Chiral Vector.

m0	m5	m6	m7	m8	m9	m10
(9,0)	–	–	–	–	–	–
(10,0)	(5,5)	–	–	–	–	–
(11,0)		–	–	–	–	–
(12,0)		(6,6)	–	–	–	–
(13,0)			–	–	–	–
(14,0)			(7,7)	–	–	–
(15,0)				–	–	–
(16,0)				(8,8)	–	–
(17,0)					–	–
(18,0)					(9,9)	–
(19,0)						–
(20,0)						(10,10)

The recommended format for the PT of the (n,m) SWNTs is presented in Table 2. The SWNTs are classified by both n and m, *e.g.*, group m0 (m = 0) includes the (n,0) SWNTs; group m5 (m = 5) comprises the (n,5) SWNTs. Periods of (n + 1)/2 (n odd) and (n + 2)/2 (n even) units are assumed because $n \geq m$. SWNTs in the same row (period) of Table 2 show close $<\alpha>$ value in Table 1.

The variation of the calculated $<\alpha>$ *vs*. n (Figure 1) suggests discontinuities for the (n,0) SWNTs with n values of 9, 10 and 11 (group m0). The distance in n units between each pair of consecutive discontinuities is 1, value that coincides with those given previously for the SWNT sets belonging to the same group in the PT (Table 2). In particular the $<\alpha>$ value for (10,10) is slightly smaller than that for the (17,0) SWNT, and rather smaller than that for (18,0) and than those extrapolated for (19,0) and (20,0) SWNTs. Of all possible SWNTs (10,10) is special. The propensity for bonding that causes C_{60} to be the end point of 30–40% of all the reactive kinetics leads to this (10,10) SWNT. Therefore, the (10,10) SWNT presents a consistency between a relatively small $<\alpha>$ and great kinetic stability.

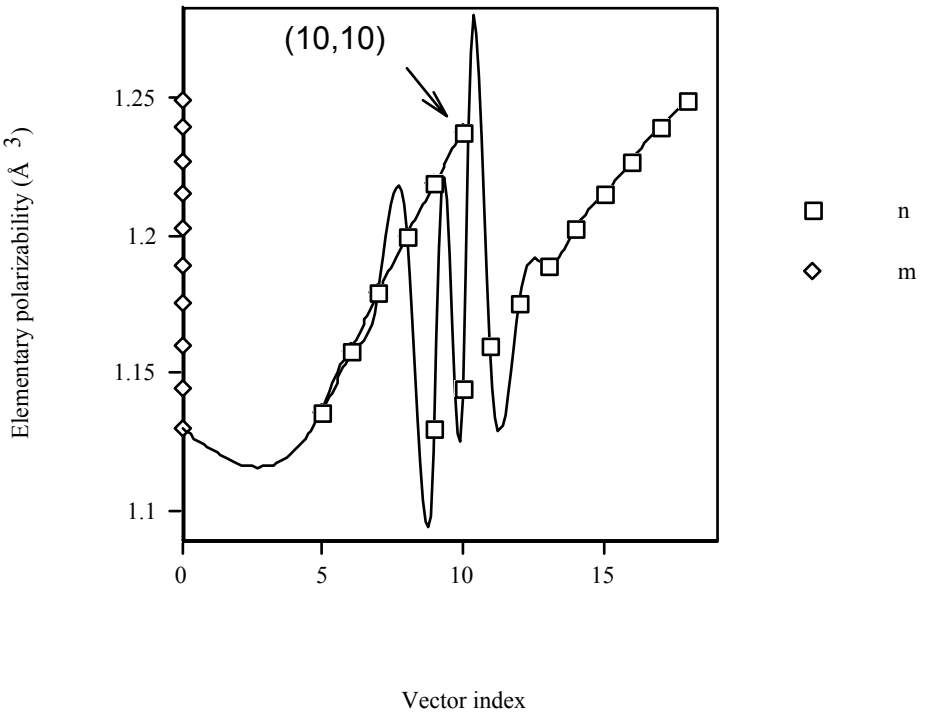

Figure 1. Variation of calculated elementary polarizability <α> *vs*. vector indices $n + m$.

The variation of the calculated <α> *vs*. $n + m$ (Figure 2) suggests discontinuities for the (n,0) SWNTs with n values of 10, 12, 14, 16 and 18 (group m0). The distance in {n,m} units between each pair of consecutive discontinuities is 2, value that coincides with those given previously for the SWNT sets belonging to the same period in the PT (Table 2). Of course the <α> value for (10,10) is slightly smaller than that for the (17,0) and (18,0) SWNTs.

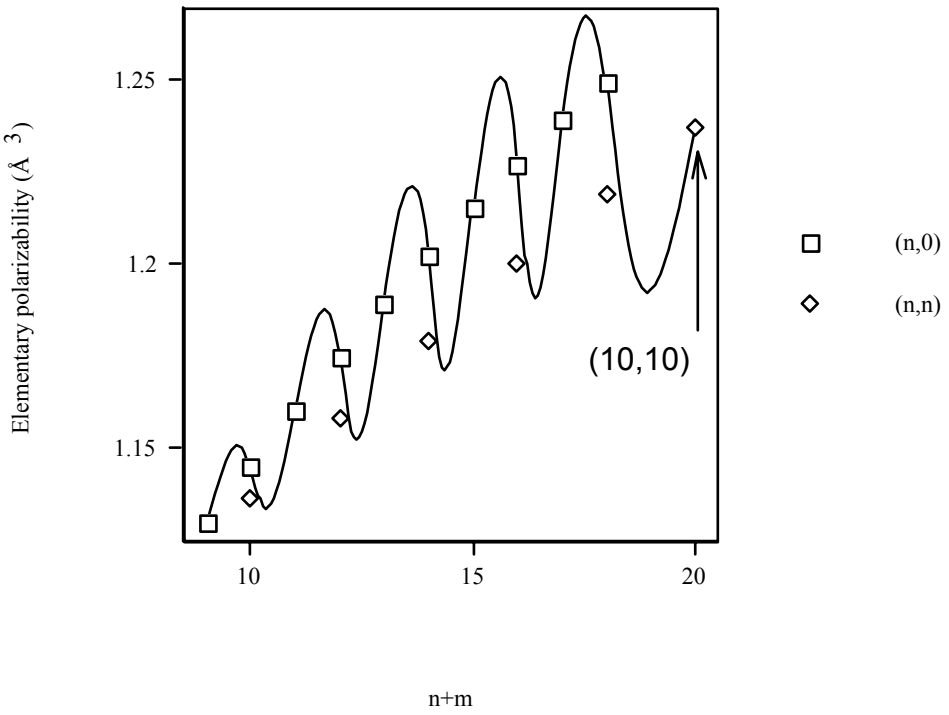

Figure 2. Variation of calculated elementary polarizability <α> *vs*. $n + m$.

Figure 3 illustrates the calculated <α> for (n,0) and (n,n) SWNTs *vs*. $(n^2+nm+m^2)^{1/2}$. Both representations correlate well with $(n^2+nm+m^2)^{1/2}$. In particular the slope for the (n,0) is slightly greater than that for the (n,n) SWNTs. For thinner SWNTs, <α> for the (n,0) C_{100}–C_{200} is calculated smaller than for the (n,n) SWNTs C_{90}–C_{180}. However this trend is reversed after R = 5.4Å for (14,0) and thicker SWNTs. For the (n,0) zigzag SWNTs C_{90}–C_{180} the variation of <α> with $(n^2+nm+m^2)^{1/2}$ fits to

$$\langle\alpha\rangle = 1.01 + 0.0133\left(n^2 + nm + m^2\right)^{1/2} \qquad N = 10 \qquad r = 0.998 \qquad s = 0.002 \qquad F = 2427.4 \tag{13}$$

For the (n,n) armchair SWNTs C_{100}–C_{200} the variation of <α> with $(n^2+nm+m^2)^{1/2}$ fits to

$$\langle\alpha\rangle = 1.04 + 0.0117\left(n^2 + nm + m^2\right)^{1/2} \qquad N = 6 \qquad r = 0.999 \qquad s = 0.002 \qquad F = 2968.6 \tag{14}$$

The <α> value for (10,10) is: (1) slightly smaller than that interpolated from the fit to the (n,n) SWNTs (Equation 14), (2) slightly smaller than that for the closer (17,0) SWNT, and (3) rather smaller than that for the (18,0) and than those extrapolated for the (19,0) and (20,0) SWNTs. Again, (10,10) presents a consistency between a relatively small <α> and great kinetic stability.

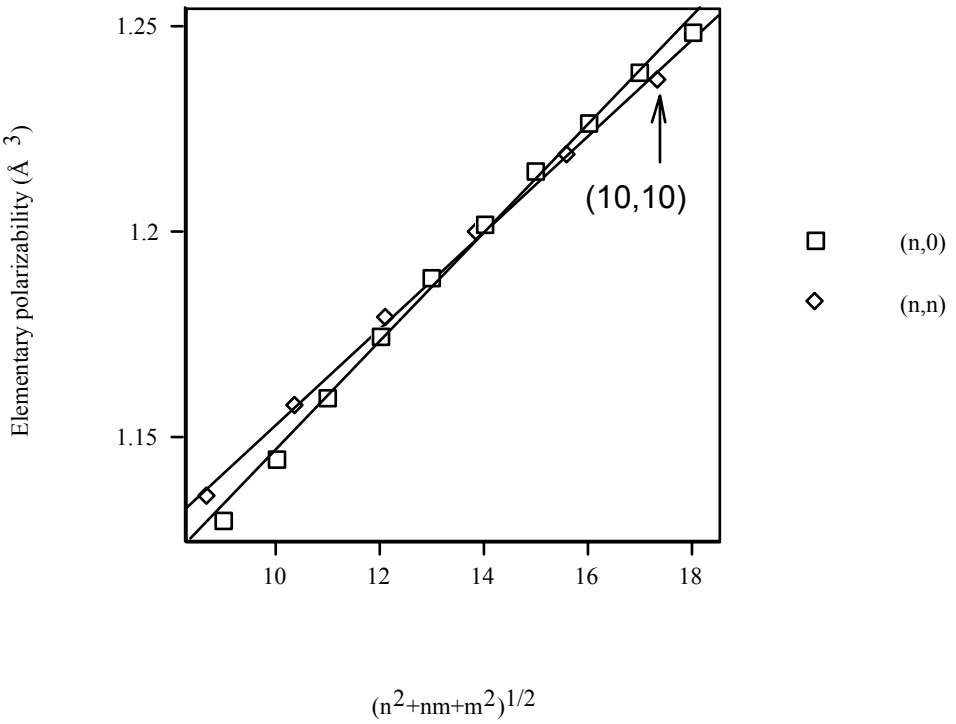

Figure 3. Variation of calculated elementary polarizability <□> *vs*. $(n^2 + nm + m^2)^{1/2}$.

If a function $<\alpha>(p)$ is assumed for a given position in the PT (Table 2), p, a maximum value of such a function $<\alpha>_{max}(p)$ for a given value of p has meaning only if it is compared with those for the former $<\alpha>(p-1)$ and later $<\alpha>(p+1)$ points, needing to fulfil:

$$\begin{aligned} \langle\alpha\rangle_{max}(p) &> \langle\alpha\rangle(p-1) \\ \langle\alpha\rangle_{max}(p) &> \langle\alpha\rangle(p+1) \end{aligned} \tag{15}$$

Conditions (15) are order relationships, being these connections precisely what, the periodic law (PL) being fulfilled rigorously, should repeat at determined intervals and equal to the values of the size of the periods. Expressions (15) are equivalent to:

$$\begin{aligned} \langle\alpha\rangle_{max}(p) - \langle\alpha\rangle(p-1) &> 0 \\ \langle\alpha\rangle(p-1) - \langle\alpha\rangle_{max}(p) &< 0 \end{aligned} \tag{16}$$

As expressions (16) are valid only for the maxima of $<\alpha>(p)$, more general others are desired for all the values of p. For that, it is considered adequate to calculate the differences $<\alpha>(p+1) - <\alpha>(p)$, assigning each of their values to SWNT p. Naming this value $D(p)$, one has:

$$D(p) = \langle\alpha\rangle(p+1) - \langle\alpha\rangle(p) \tag{17}$$

Instead of $D(p)$ the values $R(p) = <\alpha>(p+1)/<\alpha>(p)$ can be taken assigning them to SWNT p. If the PL were general, the elements belonging to the same group will satisfy, without exceptions, identical relationship:

$$D(p) > 0 \text{ or } D(p) < 0 \tag{18}$$

$$R(p) > 1 \text{ or } R(p) < 1 \quad (19)$$

However, the results show that this is not the case, so that the PL is not general, existing some anomalies, *e.g.*, the variation of $D(p)$ *vs*. p shows the lack of coherence between the Cartesian and PT representations of $<\alpha>$. If coherence were rigorous, all the points in each period will have the same sign. There is a tendency in the points to give $D(p) > 0$. However, in detail there are anomalies in the SWNTs of the successive periods. The same happens for the variation of $R(p)$ *vs*. p. If coherence were rigorous, all the points in each period will be either lower or greater than one. There is a tendency in the points to give $R(p) > 1$. Again there are anomalies in the SWNTs of the successive periods.

5 CONCLUSIONS

From the preceding results the following conclusions can be drawn.

1. Several criteria have been selected to reduce the analysis to a manageable quantity of structures from the enormous set of SWNT isomers. They refer to the chiral vector indices (n,m). The PL has not the rank of the laws of physics. (1) The properties of the SWNTs are not repeated; perhaps their chemical character. (2) The order relationships are repeated with exceptions. The analysis forces the statement: *The relationships that any SWNT* (n,m) *has with its neighbour* (n–1,m+1) *are approximately repeated for each period*. Periodicity is not general; however, if a natural order of SWNTs is accepted, the law must be phenomenological. The (9,0) and (5,5) SWNTs, which join smoothly to a C_{60} hemisphere, are the smallest diameter SWNTs that can be properly capped. This suggests that semifullerene C_{30} or higher could be the origin of every SWNT. The formation of SWNTs in carbon vapour can be acknowledged by the mechanism: $C_{\text{semifullerene}} \rightarrow C_{\text{semifullerenic SWNTlet}} \rightarrow C_{\text{fullerenic SWNT}}$. Therefore *hemispheric* semifullerenes, *e.g.*, C_{30}, can be considered as the element zero of such a PT.

2. The observed correlation between $<\alpha>$ and $(n^2+nm+m^2)^{1/2}$ shows that the vector indices (n,m), which have been used to built the PT are adequate. The most interesting index combination is $(n^2+nm+m^2)^{1/2}$.

3. The (10,10) is the most favourite SWNT. The propensity for bonding that causes C_{60} to be the end of 30–40% of all the reactive kinetics leads to (10,10). The (10,10) presents a consistency between a relatively small $<\alpha>$ and great kinetic stability.

Work is in progress on the study of the periodicity of other SWNT properties as diameter, pyramidalization angle, fractal dimension of the solvent-accessible surface, fractal dimension of the internal cavity, solubility and partition coefficients. This would give an insight into a possible generality of these conclusions.

Acknowledgment

The author acknowledges financial support from the Spanish MCT (Plan Nacional I+D+I, Project No. BQU2001-2935-C02-01).

6 REFERENCES

[1] D. Mendeleev, *The Principles of Chemistry*, Longmans and Green, London, 1905.
[2] P. Pyykkö, Relativistic Effects in Structural Chemistry, *Chem. Rev*. **1988**, *88*, 563-594.
[3] M. Randi≈ and C. L. Wilkins, Graph Theoretical Ordering of Structures as a Basis for Systematic Searches for Regularities in Molecular Data, *J. Phys. Chem*. **1979**, *83*, 1525-1540.
[4] M. Randi≈ and C. L. Wilkins, Graph-Theoretical Analysis of Molecular Properties. Isomeric Variations in Nonanes, *Int. J. Quantum Chem*. **1980**, *18*, 1005-1027.
[5] L. Bytautas and D. J. Klein, Formula Periodic Table for the Isomer Classes of Acyclic Hydrocarbons – Enumerative and Asymptotic Characteristics, *Croat. Chem. Acta* **2000**, *73*, 331-357.
[6] L. Bytautas, D. J. Klein, and T. G. Schmalz, All Acyclic Hydrocarbons: Formula Periodic Table and Property Overlap Plots *via* Chemical Combinatorics, *New J. Chem*. **2000**, *24*, 329-336.
[7] J. R. Dias, A Periodic Table for Polycyclic Aromatic Hydrocarbons, *Acc. Chem. Res*. **1985**, *18*, 241-248.
[8] J. R. Dias, A Formula Periodic Table for Benzenoid Hydrocarbons and the Aufbau and Excised Internal Structure Concepts in Benzenoid Enumerations, *J. Math. Chem*. **1990**, *4*, 17-29.
[9] D. J. Klein and W. A. Seitz, Pauling–Wheland Resonance Theory of Benzenoid Hydrocarbons, *J. Mol. Struct. (Theochem)* **1988**, *169*, 167-181.
[10] X. Liu, D. J. Klein, T. G. Schmalz, and W. A. Seitz, Generation of Carbon-Cage Polyhedra, *J. Comput. Chem*. **1991**, *12*, 1252-1259.
[11] X. Liu, D. J. Klein, W. A. Seitz, and T. G. Schmalz, Sixty-Atom Carbon Cages, *J. Comput. Chem*. **1991**, *12*, 1265-1269.
[12] A. T. Balaban, Theoretical Examination of New Forms of Carbon Formed by Intra- or Intermolecular Dehydrogenation of Polycyclic Aromatic Hydrocarbons, Particularly Helicenes, *Polycycl. Arom. Compounds* **2003**, *23*, 277-296.
[13] J. P. Corriou, O. Iordache, and D. Tondeur, Classification of Biomolecules by Information Entropy, *J. Chim. Phys. Phys.-Chim. Biol*. **1991**, *88*, 2645-2652.
[14] R. E. Smalley, From Dopyballs to Nanowires, *Mater. Sci. Eng., B* **1993**, *19*, 1-7.
[15] E. G. Gamaly and T. W. Ebbesen, Mechanism of Carbon Nanotube Formation in the Arc Discharge, *Phys. Rev. B* **1995**, *52*, 2083-2089.
[16] H. W. Kroto, J. R. Heath, S. C. O'Brien, R. F. Curl, and R. E. Smalley, C_{60}: Buckminsterfullerene, *Nature (London)* **1985**, *318*, 162-163.
[17] W. Krätschmer, L. D. Lamb, K. Fostiropoulos, and D. R. Huffman, Solid C_{60}: A New Form of Carbon, *Nature (London)* **1990**, *347*, 354-358.
[18] E. A. Rohlfing, D. M. Cox, and A. Kaldor, Production and Characterization of Supersonic Carbon Cluster Beams, *J. Chem. Phys*. **1984**, *81*, 3322-3330.
[19] E. G. Gamaly and L. T. Chadderton, Fullerene Genesis by Ion Beams, *Proc. R. Soc. London, A* **1995**, *449*, 381-409.
[20] L. T. Chadderton and E. G. Gamaly, *Nucl. Instrum. Meth., Sect. B* **1995**, *117*, 375.
[21] L. T. Chadderton and Y. Chen, Nanotube Growth by Surface Diffusion, *Phys. Lett. A* **1999**, *263*, 401-405.
[22] A. Thess, R. Lee, P. Nikolaev, H. Dai, P. Petit, J. Robert, C. Xu, Y. H. Lee, S. G. Kim, A. G. Rinzler, D. T. Colbert, G. E. Scuseria, D. Tománek, J. E. Fischer, and R. E. Smalley, Crystalline Ropes of Metallic Carbon Nanotubes, *Science* **1996**, *273*, 483-487.
[23] F. Torrens, Table of Periodic Properties of the Fullerenes Based on Structural Parameters, *J. Chem. Inf. Comput. Sci*., in press.
[24] F. Torrens, Table of Periodic Properties of Fullerenes Based on Structural Parameters *J. Mol. Struct. (Theochem)*, submitted for publication.
[25] B. T. Thole, Molecular Polarizabilities Calculated with a Modified Dipole Interaction, *Chem. Phys*. **1981**, *59*, 341-350.
[26] K. J. Miller, Calculation of the Molecular Polarizability Tensor, *J. Am. Chem. Soc*. **1990**, *112*, 8543-8551.
[27] C. Voisin and A. Cartier, Determination of Distributed Polarizabilities to Be Used for Peptide Modeling, *J. Mol. Struct. (Theochem)* **1993**, *286*, 35-45.
[28] N. L. Allinger, Conformational Analysis. 130. MM2. A Hydrocarbon Force Field Utilizing V_1 and V_2 Torsional Terms, *J. Am. Chem. Soc*. **1977**, *99*, 8127-8134.

[29] J. A. Deiters, J. C. Gallucci, T. E. Clark, and R. R. Holmes, Computer Simulation of Phosphorane Structures, *J. Am. Chem. Soc*. **1977**, *99*, 5461-5471.
[30] G. Némethy, M. S. Pottle, and H. A. Scheraga, Energy Parameters in Polypeptides. 9. Updating of Geometric Parameters, Nonbonded Interactions, and Hydrogen Bond Interactions for the Naturally Occurring Amino Acids, *J. Phys. Chem*. **1983**, *87*, 1883-1887.
[31] F. Torrens, M. Ruiz-López, C. Cativiela, J. I. García, and J. A. Mayoral, Conformational Aspects of Some Asymmetric Diels-Alder Reactions. A Molecular Mechanics + Polarization Study, *Tetrahedron* **1992**, *48*, 5209-5218.
[32] F. Torrens, Nature of Fe^{III}–O_2, Fe^{II}–CO and Fe^{III}–CN Complexes of Hemoprotein Models, *Polyhedron* **2003**, *22*, 1091-1098.
[33] F. Torrens, Polarization Force Fields for Peptides Implemented in ECEPP2 and MM2, *Mol. Simul*. **2000**, *24*, 391-410.
[34] F. Torrens, Effect of Elliptical Deformation on Molecular Polarizabilities of Model Carbon Nanotubes from Atomic Increments, *J. Nanosci. Nanotech*. **2003**, *3*, 313-318.
[35] F. Torrens, Effect of Size and Deformation on Polarizabilities of Carbon Nanotubes from Atomic Increments, *Future Generation Comput. Syst*., in press.
[36] L. Jensen, O. H. Schmidt, K. V. Mikkelsen, and P.-O. Åstrand, Static and Frequency-Dependent Polarizability Tensors for Carbon Nanotubes, *J. Phys. Chem. B* **2000**, *104*, 10462-10466.
[37] X. Blasé, L. X. Benedict, E. L. Shirley, and S. G. Louie, Hybridization Effects and Metallicity in Small Radius Carbon Nanotubes, *Phys. Rev. Lett*. **1994**, *72*, 1878-1881.
[38] S. Niyogi, M. A. Hamon, H. Hu, B. Zhao, P. Bhowmik, R. Sen, M. E. Itkis, and R. C. Haddon, Chemistry of Single-Walled Carbon Nanotubes, *Acc. Chem. Res*. **2002**, *35*, 1105-1113.
[39] D. H. Robertson, D. W. Brenner, and J. W. Mintmire, Energetics of Nanoscale Graphitic Tubules, *Phys. Rev. B* **1992**, *45*, 12592-12595.

Biography

Francisco Torrens is lecturer of physical chemistry at the Universitat de València. After obtaining a Ph.D. degree in molecular associations in azines and macrocycles from the Universitat de València, Dr. Torrens undertook postdoctoral research with Professor Rivail at the Université de Nancy I. More recently, Dr. Torrens has collaborated on projects with Professor Tomás-Vert. Major research projects include characterization of the electronic structure of electrically conductive organic materials, theoretical study of new electrically conductive organic materials, modellization of proteins, electronic correlation, development and applications of high-precision mono and multireferential electronic correlation methods, and development and application of high-precision quantum methods. Scientific accomplishments include the first implementation in a computer at the Universitat de Valencia of a program for the elucidation of crystallographic structures, and the construction of the first computational-chemistry program adapted to a vector-facility supercomputer at a Spanish university.